Available online at www.sciencedirect.com
ScienceDirect
International Journal of Heat and Mass Transfer 51 (2008) 4069–4082
International Journal of HEAT and MASS TRANSFER
www.elsevier.com/locate/ijhmt

Modeling of the microconvective contribution to wall heat transfer in subcooled boiling flow

Franz Ramstorfer [a,1], Helfried Steiner [b,*], Günter Brenn [b,2]

[a] The Virtual Vehicle Competence Center, Inffeldgasse 21A, 8010 Graz, Austria
[b] Institute of Fluid Mechanics and Heat Transfer, Graz University of Technology, Inffeldgasse 25F, 8010 Graz, Austria

Received 5 March 2007; received in revised form 10 September 2007
Available online 29 January 2008

Abstract

In the present work, the two-phase turbulent boundary layer in subcooled boiling flow is investigated. The bubbles in the near-wall region have a significant effect on the dynamics of the underlying liquid flow, as well as on the heat transfer. The present work develops a single-fluid model capable of accounting for the interactions between the bubbles and the liquid phase, such that the two-phase convective contribution to the total wall heat transfer can be described appropriately even in the framework of single-fluid modeling. To this end, subcooled boiling channel flow was experimentally investigated using a laser-Doppler anemometer to gain insight into the bubble-laden near-wall velocity field. It was generally observed that the streamwise velocity component was considerably reduced compared to the single-phase case, while the near-wall turbulence was increased due to the presence of the bubbles. Since the experimentally observed characteristics of the liquid velocity field turned out to be very similar to turbulent flows along rough surfaces, it is proposed to model the near-wall effect of the bubbles on the liquid flow analogously to the effect of a surface roughness. Incorporating the proposed approach as a dynamic boundary condition into a well-established mechanistic flow boiling model makes it possible to reflect adequately the contribution of the microconvection to the total wall heat transfer. A comparison against the experimental data shows good agreement for the predicted wall shear stress as well as for the wall heat flux for a wide range of wall temperatures and Reynolds numbers.

Keywords: Subcooled boiling flow; Turbulent boundary layer; Modified law of the wall; Microconvection

1. Introduction

A reliable mathematical description of the correlation between the local wall superheat and the heat flux across a heated surface in subcooled flow boiling is becoming increasingly important for the design of highly efficient liquid cooling systems. A large number of wall heat flux models [1–3,8–13] have been proposed in the past and are still further developed. Due to the high complexity of the problem involving a great variety of thermophysical effects, which are often hard or even impossible to measure, no rigorous analytical description of the nucleate boiling process has been derived yet. Therefore, most state-of-the-art models rely on a good deal of empiricism in terms of adjustable model parameters.

A certain class of models assumes the total wall heat flux q_w as a single-phase convective heat flux enhanced by a factor. Models of this type, as proposed by, e.g., Kandlikar [1] and Shah [2], write the total wall heat flux q_w generally as the product:

$$q_w = q_{conv,1ph}\psi_{2ph}, \tag{1}$$

where $q_{conv,1ph}$ represents the single-phase convective heat flux, which is multiplied by an enhancement factor ψ_{2ph}. The enhancement factor is in general modeled as a function of the Boiling number Bo, such that

* Corresponding author. Tel.: +43 316 873 7344; fax: +43 316 873 7356.
E-mail addresses: franz.ramstorfer.ext@siemens.com (F. Ramstorfer), steiner@fluidmech.tu-graz.ac.at (H. Steiner), brenn@fluidmech.tu-graz.ac.at (G. Brenn).
[1] Tel.: +43 732 6592 74347; fax: +43 732 6980 2047.
[2] Tel.: +43 316 873 7340; fax: +43 316 873 7356.

0017-9310/$ - see front matter © 2008 Elsevier Ltd. All rights reserved.
doi:10.1016/j.ijheatmasstransfer.2007.10.039

Nomenclature

Bo	Boiling number (–)
c	specific heat capacity of the liquid (J/kg K)
C	integration constant (–)
C_{kr}	roughness constant (–)
C_{krc}	roughness constant (–)
C_{sf}	parameter (–)
d	bubble diameter (m)
D_h	hydraulic diameter (m)
Ec	Eckert number (–)
F_{2ph}	enhancement factor (–)
Fr	Froude number (–)
g	gravitational acceleration (m/s^2)
h_{lg}	specific latent heat of evaporation (J/kg)
Ja	Jakob number (–)
k_r	physical roughness height (m)
$\tilde{k}_r$	modeled roughness height (m)
m	model constant (–)
$\dot{m}$	mass flux (kg/m^2 s)
p	pressure (bar)
q	heat flux (W/m^2)
Re	Reynolds number (–)
Re_b	bubble Reynolds number (–)
S	suppression factor (–)
T_{sat}	saturation temperature (K)
ΔT_{sub}	$T_{sat} - T_b$ subcooling (K)
ΔT_w	$T_w - T_{sat}$ wall superheat (K)
u	velocity component in the streamwise direction (m/s)
u_τ	$\sqrt{\tau_w/\rho_l}$ wall friction velocity (m/s)
v	velocity component in the wall-normal direction (m/s)
x	cartesian coordinate in the streamwise direction (mm)
x_v	mass fraction of vapor (–)
y	distance from the heated wall (m)

Greek symbols

γ	model parameter (–)
δ	model parameter (–)
Δ	difference
ε	convergence criterion (–)
$\bar{\varepsilon}$	turbulent dissipation rate (m^2/s^3)
ζ	model parameter (–)
η	model parameter (–)
κ	von Kármán constant (–)
λ_f	friction coefficient (–)
μ	dynamic viscosity of the liquid (kg/m s)
ν	kinematic viscosity of the liquid (m^2/s)
ρ	density (kg/m^3)
σ	surface tension (N/m)
τ	shear stress (N/m^2)
τ_{drag}	bubble relaxation time (s)
τ_{flow}	turbulent flow time scale (s)
Ψ_{2ph}	enhancement factor (–)

Subscripts

b	bulk
conv	convective
l	liquid
m	median
nb	nucleate boiling
rms	root mean square
v	vapor
w	wall
1ph	single-phase
2ph	two-phase

Superscript

+	quantities in wall units

$$\psi_{2ph} = \psi_{2ph}(Bo) \quad \text{with } Bo = \frac{q_w}{\dot{m} h_{fg}}. \tag{2}$$

The essential shortcoming of this class of models arises when approaching the limit of pool boiling, since the Boiling number goes by definition to infinity for vanishing mass fluxes $\dot{m}$.

An alternative approach to the multiplicative concept of Eq. (1) is represented by the superposition models. This widely used concept, which was introduced by Chen [3], assumes the total wall heat flux to be additively composed of a macroscopic, convective component and a microscopic, nucleate boiling component, such that one may write

$$q_w = q_{conv,1ph} F_{2ph} + q_{nb} S. \tag{3}$$

This linear decomposition is attractive for two reasons. First, it offers much freedom in choosing most adequate submodels for each component. Secondly, it provides the correct asymptotics at the transition to the non-boiling regime, where the nucleate boiling component q_{nb} becomes zero and only the macroscopic, single-phase convection $q_{conv,1ph}$ remains. The macroscopic component is mostly obtained from typical textbook correlations for forced convective channel flows, such as the Dittus–Boelter correlation. The microscopic contribution is generally computed using well-established pool boiling models, such as those proposed by Forster and Zuber [4], Cooper [5], Gorenflo [6], or Rohsenow [7]. The factor S in Eq. (3) represents a flow-induced suppression of the nucleate boiling component. It is often modeled as a function of the flow Reynolds Re number decreasing from $S = 1$ to $S = 0$ for increasing

Re. The factor F_{2ph} represents the enhancement of the single-phase convective component by the bubble agitation. It is generally correlated as mainly dependent of the mass fraction of the vapor, such that $F_{2ph} = F_{2ph}(x_v)$.

Chen's concept was adopted by many authors using different submodels for the pool boiling heat flux and various correlations for the suppression factor S [8–11].

Extending an ansatz originally proposed by Kutateladze [12], Steiner and Taborek [13] replaced Chen's linear superposition by a non-linear or so-called power-additive superposition

$$q_w = [(q_{conv,1ph}F_{2ph})^m + q_{nb}^m]^{1/m}, \quad m > 1. \tag{4}$$

While a two-phase convection enhancement factor F_{2ph} is incorporated as well, a flow-induced suppression factor S is not required here, because the non-linear addition inherently gives more weight to that component, which becomes dominant in each asymptotic limit, and, hence, suppresses the other.

The fact that the enhancement factor is mostly obtained as function of the mass fraction of the vapor, $F_{2ph} = F_{2ph}(x_v)$, imposes a serious practical difficulty in the case of subcooled boiling flow. In this regime the vapor bubbles exist only in a very confined superheated layer close to the wall, which makes it difficult to measure the mass fraction of the vapor as a reliable input parameter to these models. For this reason many authors simply neglect the effect of the bubbles on the convection by setting the two-phase convection enhancement factor to unity, $F_{2ph} = 1$. On the other hand, flow boiling experiments such as those carried out by Maurus [14] demonstrated clearly a significant influence of the bubbles on the liquid flow field, also in the case of subcooled boiling flow.

In the present work subcooled boiling flow experiments are carried out with varying wall heat flux and flow Reynolds number. In these experiments, the near-wall velocity field is closely investigated using a laser-Doppler anemometer, which allows for the measurement of the mean velocity profiles as well as the profiles of the turbulent fluctuations of the liquid phase. Based on the experimental findings, a wall model is proposed, which reflects adequately the experimentally observed features of the near-wall flow for use in a single-fluid modeling of the total wall heat flux.

The present article is organized as follows. In Section 2, the experimental apparatus is described. In Section 3, the results obtained in the subcooled boiling flow experiments are presented and discussed. The modeling of the streamwise velocity component and the total wall heat flux is presented in Section 4. The limits of the proposed model approach are examined in Section 5. The conclusions are given in Section 6.

2. Experimental setup

The experimental facility, which is sketched in Fig. 1, basically consists of a closed loop channeling a forced convective flow driven by a pump. The working fluid passes through a heated test section, which is schematically shown in Fig. 2. The bulk velocity, the bulk liquid temperature, and the operating pressure at the inlet of the section are controlled. In the present configuration, the bulk velocity may be varied within the range of $0.05\ \text{m/s} \leqslant u_b \leqslant 2.0\ \text{m/s}$, which corresponds to a range of flow Reynolds numbers between 5629 and 112,580. The absolute operating pressure can be set within the range $1.0\ \text{bar} \leqslant p \leqslant 2.0\ \text{bar}$. The square-shaped cross section of the test section has the dimensions 36 mm × 36 mm. The heat transfer to the flowing liquid is provided by electrically heated coils located at the bottom of the aluminum heater from where the heat is conducted to the heater surface. The heater surface (grey shaded in Fig. 2), which is the heated area of the test

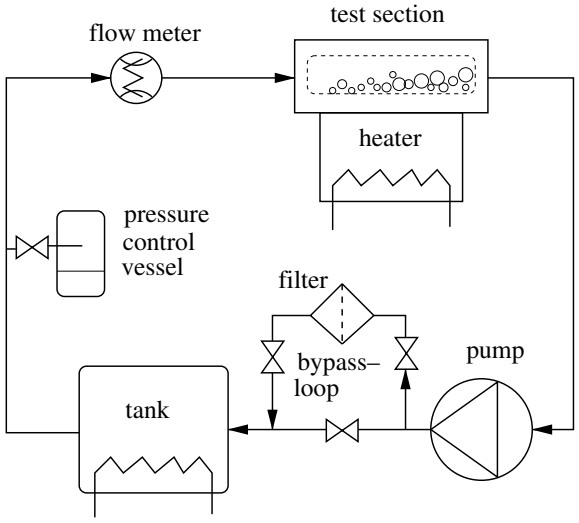

Fig. 1. Schematic diagram of the convective boiling flow loop.

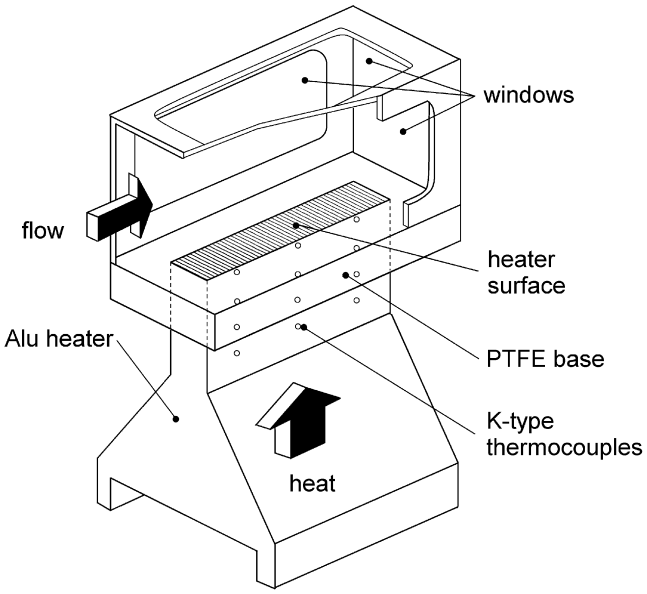

Fig. 2. Test section of the experimental facility.

section with a streamwise length of 65 mm and a width of 10 mm.

The wall temperature and the wall heat flux are determined based on Fourier's law of heat conduction using the temperatures measured with twelve K-type thermocouples appropriately distributed in the solid heater. The position of the individual thermocouples can be seen from Fig. 2. The base plate of the test section, where the top of the aluminum heater is embedded, is made of polytetrafluoroethylene (PTFE). The very low thermal conductivity of PTFE should guarantee the lowest possible heat loss from the heater material to the surrounding structure. Due to thermal durability restrictions of the PTFE base plate, the maximum heater surface temperature was limited to $T_w = 160\ ^\circ C$. One important aspect is the role of this base plate for tightening the test section. Windows made of glass are embedded in the top as well as in the side walls of the test section to make the section optically accessible.

The size and motion of the bubbles were recorded using a high-speed camera (model: KODAK Motion Corder SR-1000C). A 2D laser-Doppler anemometer from DANTEC (wavelengths 514.5 nm and 488 nm, focal length 310 mm, beam spacing 60 mm) was used for the liquid velocity measurements. Laser-Doppler anemometry has become a well-established technique for local velocity measurements in transparent single-phase flows because of its high accuracy, good spatial and temporal resolution, and non-intrusive features. In general, the flow is seeded with tracer particles, which serve as scattering centers for the laser light. In the case of flow boiling experiments, no seeding particles may be added to the liquid, since they might affect the nucleate boiling process. While small, particle-like contaminations in the working liquid serve as scattering centers in the outer, single-phase region, a sufficiently high signal rate is provided by the vapor bubbles in the two-phase region. Using the vapor bubbles as tracers for the liquid flow inherently assumes the slip between the bubbles and the liquid phase to be negligibly small. The validity of this assumption was justified by comparing the bubble relaxation time based on the bubble drag force, τ_{drag}, to the relevant turbulent flow time scale, τ_{flow}. The former is estimated following Mei et al. [15]:

$$\tau_{drag} = \frac{\rho_v d_m^2}{12\mu}\left\{1 + [8/Re_b + 1/2(1 + 3.315Re_b^{-0.5})]^{-1}\right\}^{-1}, \tag{5}$$

where Re_b is the bubble Reynolds number $Re_b = d_m u_b/\nu$ using the median bubble detachment diameter d_m from the high-speed camera recordings as the length scale. The latter is estimated based on Kolmogorov's second similarity hypothesis, assuming that the bubble diameter lies well within the inertial subrange of the wavelength spectrum of turbulence, such that one may write

$$\tau_{flow} = \left(\frac{d_m^2}{\bar{\varepsilon}}\right)^{1/3}. \tag{6}$$

Here $\bar{\varepsilon}$ denotes the average dissipation rate of kinetic energy per unit mass. It is estimated in terms of the pressure loss of a turbulent channel flow, which reads

$$\bar{\varepsilon} = \frac{\Delta p}{\Delta x}\frac{u_b}{\rho} \quad \text{with} \quad \frac{\Delta p}{\Delta x} = \frac{\lambda_f}{D_h}\rho\frac{u_b^2}{2}. \tag{7}$$

Using the Blasius law for the wall friction coefficient, we have $\lambda_f = 0.316Re^{-0.25}$. The Reynolds number $Re = u_b D_h/\nu$ is based on the bulk flow quantities. In all considered cases the turbulent flow time scale turned out to be about three orders of magnitude smaller than the bubble relaxation time such that $\tau_{drag}/\tau_{flow} \ll 1$. This indicates clearly that the bubbles accurately follow the turbulent liquid motion and are therefore suitable as tracers for the LDA measurements.

The maximum total error relative to the measured heat flux is estimated as $\pm 5\%$ in the convective regime and $\pm 2\%$ in the nucleate boiling regime. The error in the measured surface temperatures is ± 0.15 K. The inductive flow meter measures the bulk velocity with a relative error of $\pm 0.5\%$ of the displayed value.

3. Experimental conditions and results

In all our experiments, the working fluid was a mixture ethylene glycol/water in a volumetric composition of 40/60 vol.%. The absolute system pressure $p = 1.5$ bar, as well as the subcooling $\Delta T_{sub} = T_{sat} - T_b = 22$ K were kept constant in all experiments. The wall heat flux q_w was varied between very low values and a maximum of about 500 kW/m^2, leading to a maximum wall superheat of about $\Delta T_w = T_w - T_{sat} = 40$ K. The bulk velocity of the working fluid was varied within the range of $0.1\ \text{m/s} \leqslant u_b \leqslant 0.8\ \text{m/s}$. The corresponding Reynolds number based on the bulk flow quantities ranges from 5629 to 45,030.

The heat transfer conditions of all experimentally investigated cases can be seen from Fig. 3, where the corresponding measured total wall heat flux q_w is plotted vs. the wall superheat ΔT_w. Most cases lie well inside the nucleate boiling region to the right of the saturation line $\Delta T_w = 0$. For each bulk velocity, at least one purely convective, non-boiling case, associated with $\Delta T_w < 0$, is investigated as well. The data point on the abscissa refers to the unheated reference cases without heat transfer to the liquid (denoted with $q_w = 0$) for use in the comparison with the bubble-laden, boiling cases in the discussion of the measured near-wall velocity profiles.

The results of the LDA measurements for the boiling cases and for the unheated reference case shown in Fig. 3 are displayed in Figs. 4–7. The mean values of the velocity components $\bar{u}$ and $\bar{v}$ in the streamwise and the wall-normal direction, respectively, as well as the rms-values of the corresponding fluctuations, u_{rms} and v_{rms}, are plotted against the wall-normal distance y. All displayed velocity profiles are scaled with the bulk velocity u_b. A comparison with the bubble-free reference cases ($q_w = 0$)

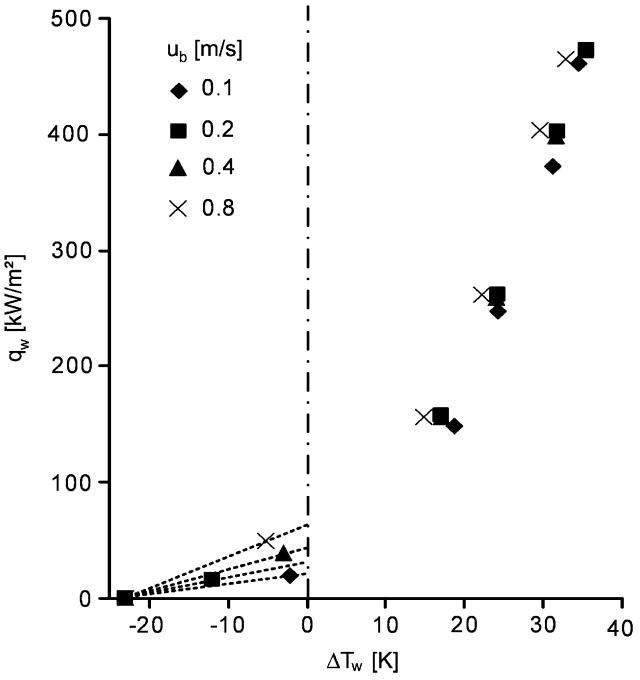

Fig. 3. Measured total wall heat flux q_w vs. the wall superheat ΔT_w at different bulk velocities u_b for $p = 1.5$ bar. The dashed lines represent the single-phase macro-convection. The dash-dotted line denotes the saturation temperature ($\Delta T_w = 0$).

makes it evident that the bubbles affect the flow considerably in the superheated near-wall layer. This influence becomes more pronounced with increasing boiling activity on the surface, as wall heat fluxes become higher. In the core flow region outside the superheated layer, the velocity profiles merge with the single-phase velocity of the non-boiling cases. Figs. 4a–7a show that in the two-phase region, the mean velocity $\bar{u}(y)$ in the streamwise direction is always significantly reduced against the non-boiling case. The presence of the vapor bubbles on the heated surface evidently generates an additional drag force on the mean flow. For continuity reasons the strongly retarded streamwise velocity is accompanied by a stronger displacement of liquid away from the wall, as indicated by the increased wall-normal component $\bar{v}(y)$ in Figs. 4b–7b. In the cases of very low bulk velocities ($u_b = 0.1$ m/s, $u_b = 0.2$ m/s) and high heat fluxes, the maximum of the mean wall-normal velocity component assumes the same order of magnitude as the streamwise component $\bar{u}(y)$, and the profiles for the streamwise component exhibit non-monotonous behavior (see Figs. 4a and 5a). With the values for $\bar{v}/u_b$ shown in Figs. 4b and 5b becoming of the order of unity, the buoyancy-induced vertical momentum is obviously of the same strength as the momentum in the streamwise direction.

As shown in Figs. 4c and d to 7c and d, the presence of the bubbles causes a marked increase of the mean turbulent fluctuations in the streamwise and the wall-normal directions, $u_{rms}(y)$ and $v_{rms}(y)$, respectively, in the two-phase region of the flow. The observed increase of the turbulent velocity fluctuations in the near-wall region leads to enhanced momentum and heat transfer. As such, the bubble-induced convective mixing strongly contributes to the total heat flux achievable in subcooled boiling flow as compared to single-phase convection.

4. Modeling

4.1. Streamwise velocity component

Most of the models proposed for the liquid velocity field in bubble-laden boundary layer flows were developed for non-boiling flow, where the gas bubbles are injected through the porous channel walls. Typical representatives are the studies of Troshko and Hassan [16] and Mikielewicz [17]. Since both approaches essentially rely on the void fraction as a key input parameter, they can hardly be extended to the subcooled boiling flow case. In contrast to the non-boiling case, where the void fraction can be determined fairly accurately from the given gas injection through the porous walls, the void fraction in the flow boiling case results from the whole process of bubble nucleation, growth, detachment, and collapse. As such, being determined by the complex interaction of various sub-processes, its estimation based on the given thermophysical conditions in the near-wall region, such as wall superheat, subcooling, pressure, etc., is inevitably affected by much uncertainty. Moreover, since the bubbles collapse once they leave the superheated wall layer, the vapor phase exists only in a thin near-wall region. Dealing with a very thin, densely populated two-phase layer makes it almost impossible to obtain reliable experimental data for the void fraction, nor when using optical, neither with intrusive methods.

The difficulty in estimating and/or measuring a relevant void fraction in subcooled boiling flow with sufficient accuracy suggested to go for an alternative approach, which was originally proposed by Gabillet et al. [18]. They also investigated the non-boiling case in a horizontal channel flow configuration, where the bubbles were injected through the porous lower channel wall. They observed that the effect of the bubbles on the liquid flow was very similar to the effect of a surface roughness. Exploiting this similarity, they proposed to capture the influence of the bubbles on the liquid flow field using a logarithmic law of the wall, which is commonly used for turbulent flows along rough walls. The bubble-equivalent roughness height required by the model was found to correlate very well with the size of the injected gas bubbles. The present work extends this similarity to subcooled boiling flow, where the bubble layer, which is generated by evaporation on the superheated wall, is assumed to act like a rough surface as well. A standard formulation for the logarithmic law of the wall for turbulent flows over rough surfaces. It reads

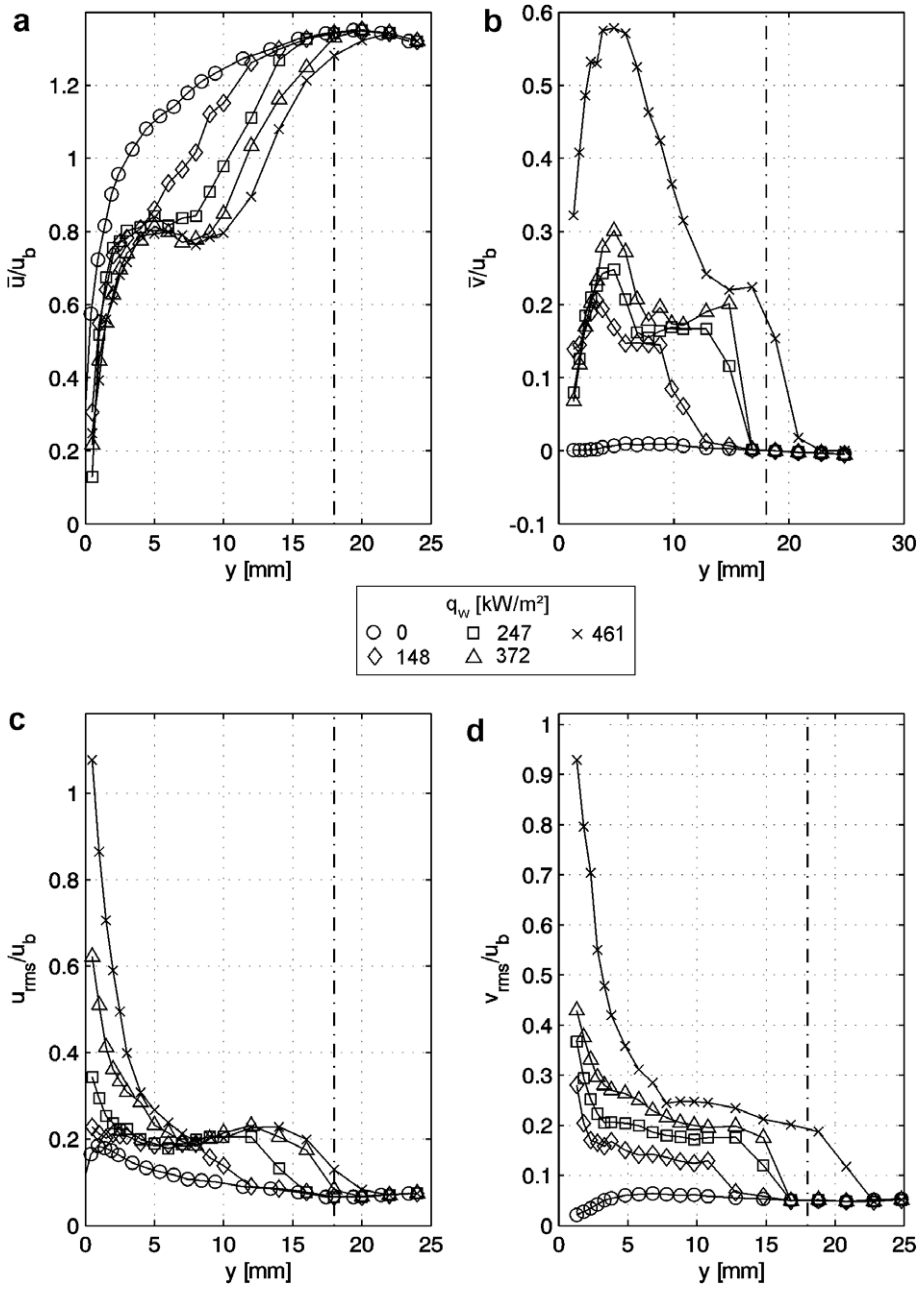

Fig. 4. Results of the LDA measurements at the bulk velocity $u_b = 0.1$ m/s for varying heat flux q_w. The dash-dotted line marks the center of the test channel.

$$u^+ = \frac{1}{\kappa}\ln y^+ + C - \Delta u^+. \tag{8}$$

Therein, $u_+ = \bar{u}/u_\tau$ and $y^+ = u_\tau y/v$ represent the wall units involving the wall friction velocity $u_\tau = \sqrt{\tau_w/\rho}$ as the relevant velocity scale. $C = 5.3$ and $\kappa = 0.41$ are constants. The last term represents the offset of u^+ due to the wall roughness with respect to the log-law for hydrodynamically smooth surfaces, where $\Delta u^+ = 0$. The offset Δu^+ on the RHS of Eq. (8) depends on the physical roughness height k_r in terms of the roughness-based Reynolds number $k_r^+ = u_\tau k_r/v$. In the specification of $\Delta u^+(k_r^+)$, a hydrodynamically smooth, a transitional, and a fully rough regime are distinguished [19]:

$$\Delta u^+ = \begin{cases} 0, & \\ & k_r^+ < 2.25, \\ \frac{1}{\kappa}\ln\left(\frac{k_r^+ - 2.25}{87.75} + C_{kr}k_r^+\right)\sin[0.426(\ln k_r^+ - 0.811)], & \\ & 2.25 \leqslant k_r^+ < 90, \\ \frac{1}{\kappa}\ln(1 + C_{kr}k_r^+), & \\ & k_r^+ \geqslant 90. \end{cases} \tag{9}$$

The roughness-type dependent constant C_{kr} is set to 0.5, which corresponds to the value commonly used for sand-grain roughness. In Fig. 8, the measured velocity profiles

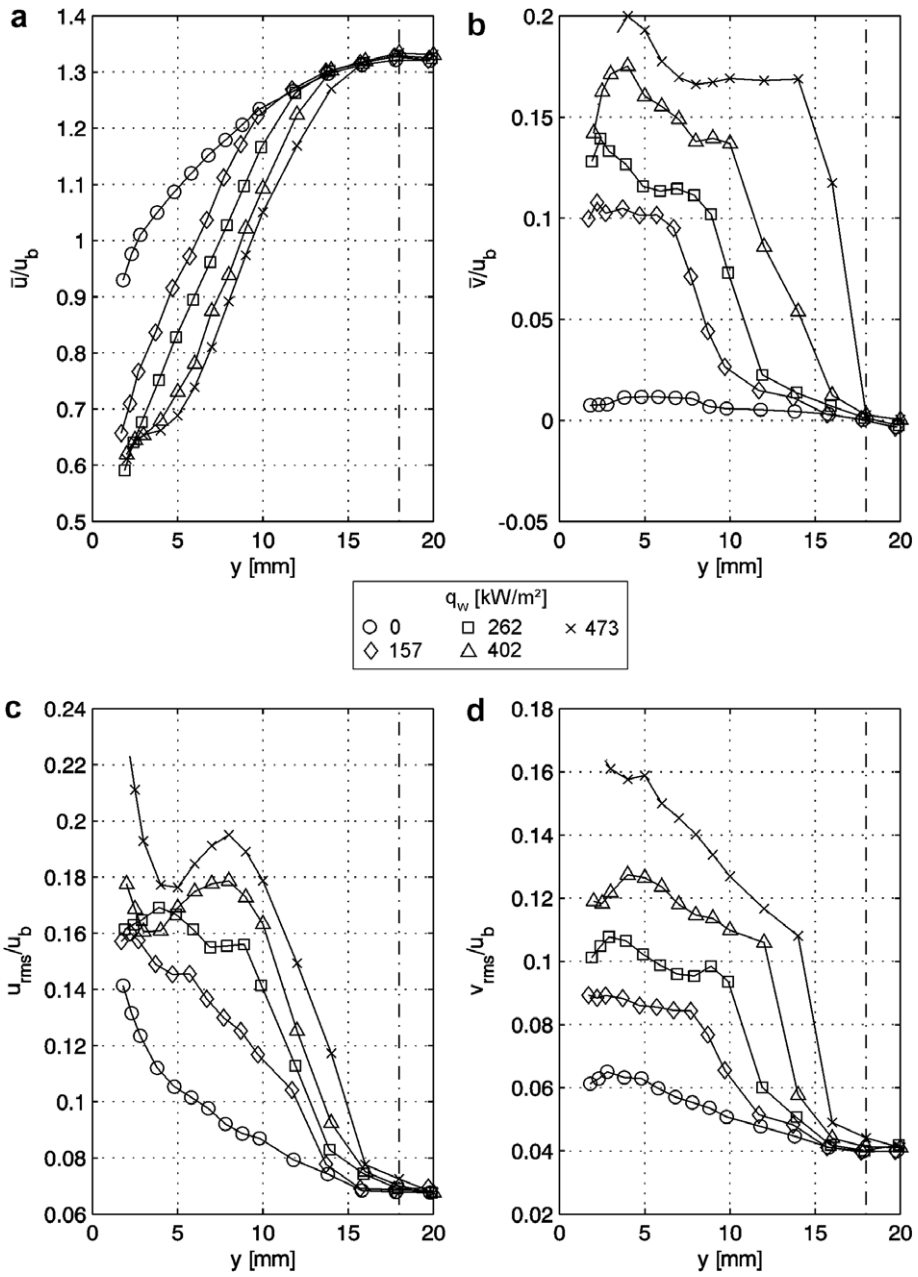

Fig. 5. Results of the LDA measurements at the bulk velocity $u_b = 0.2$ m/s for varying heat flux q_w. The dash-dotted line marks the center of the test channel.

$\bar{u}y$ shown in Figs. 4a–7a are recast into the corresponding wall coordinates as obtained by Eq. (8) using an appropriate pair of scaling parameters u_τ and k_r for each profile. The logarithmic law of the wall given by Eq. (8) evidently approximates the data very well in the range $30 < y^+ < 200$. It is noted that the profiles which exhibit a plateau in the near-wall region, as shown in Figs. 4a and 5a, had to be excluded from this analysis. In these cases, the buoyancy-induced vertical bubble motion is too strong to allow for a simple log-law modeling, which is only applicable if the motion in the main flow direction is dominant.

The roughness heights k_r fitted from the experimental data basically represent an equivalent roughness incorporating the dynamic effect of the vapor bubble layer on the liquid flow. This bubble-equivalent roughness height k_r has to be provided by an appropriate model correlation to finally determine the actual near-wall velocity profile using Eq. (8). In the proposed correlation it is assumed that the relevant length scale for the bubble-equivalent roughness height is represented by the bubble diameter d_{dep} at the instant of departure from the nucleation site. This diameter is computed following the bubble detachment model of Zeng et al. [20]. In this model, the diameter d_{dep} is obtained from a balance of drag, shear-lift, buoyancy, and bubble-growth forces. As such, the departure diameter is determined as mainly dependent on the wall superheat

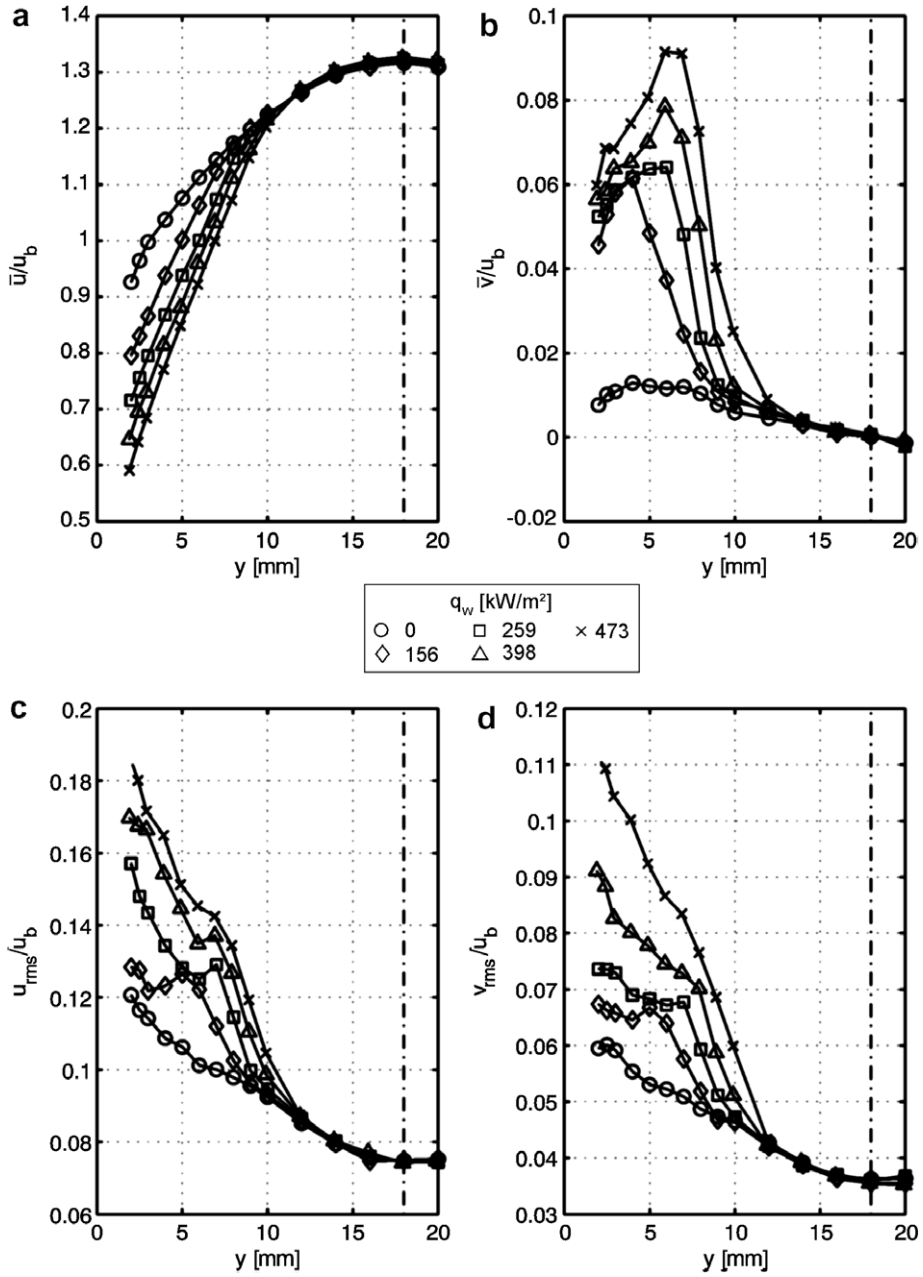

Fig. 6. Results of the LDA measurements at the bulk velocity $u_b = 0.4$ m/s for varying heat flux q_w. The dash-dotted line marks the center of the test channel.

ΔT_w and the wall friction velocity u_τ. Fig. 9 shows the diameters predicted by this detachment model compared to the corresponding experimental data obtained from the high-speed camera recordings. While the overall agreement is very good, a somewhat higher deviation is observed for the largest diameter. This can be explained by the fact that large bubble sizes basically occur at high heat fluxes and low flow velocities. For such conditions, the heated surface is in general densely populated with vapor bubbles, and the bubble departure size becomes notably affected by the bubble–bubble interactions as well. These interactions are not accounted for in the model of Zeng et al. [20], which considers only the behavior of a single bubble, leading to less accurate predictions in such a dense bubble regime. The so obtained length scale is further modified by the ratio of the nucleate boiling component to the total heat flux, q_{nb}/q_w, which represents the boiling activity, so that the proposed correlation can be written as

$$\tilde{k}_r = \eta d_{dep} \left(\frac{q_{nb}}{q_w} \right)^{\zeta}. \tag{10}$$

Evidently, as the boiling activity increases, such that q_{nb}/q_w approaches unity, the dynamic influence of the bubble layer on the liquid flow in terms of $\tilde{k}_r$ becomes highest. On the other hand, at very low nucleate boiling heat fluxes q_{nb}, associated with a heater surface sparsely populated with bubbles, the bubble influence on the liquid flow van-

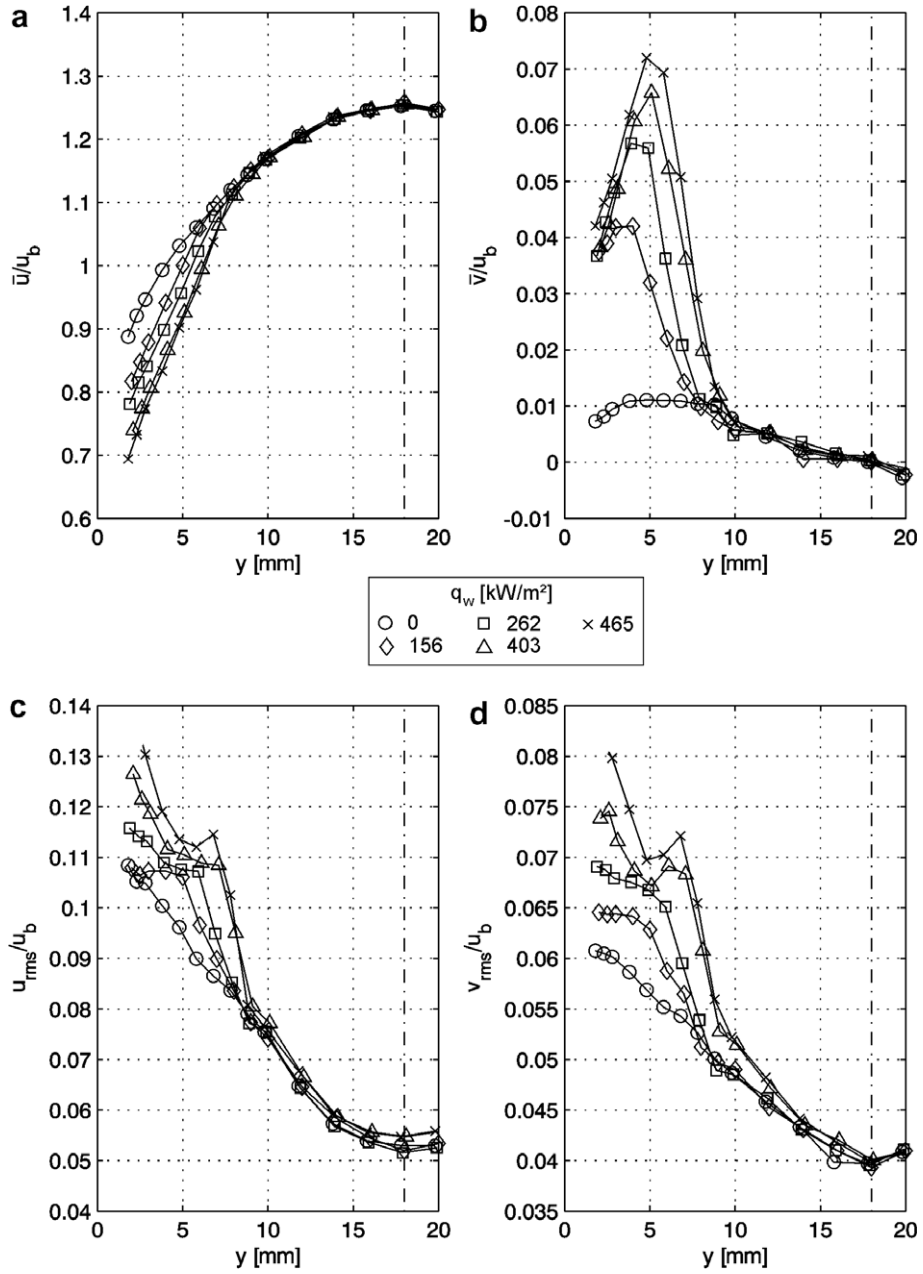

Fig. 7. Results of the LDA measurements at the bulk velocity $u_b = 0.8$ m/s for varying heat flux q_w. The dash-dotted line marks the center of the test channel.

ishes, and $\tilde{k}_r$ goes to zero. The constants η and ζ in Eq. (10) are empirical parameters, which are determined from the experimental data. The determination of the values of these parameters requires the knowledge of q_{nb}, which is very difficult to measure directly. It is therefore obtained indirectly in terms of the convective counterpart. Accordingly, assuming the classical superposition concept for the total wall heat flux q_w introduced by Chen [3], the nucleate boiling contribution can be written as

$$q_{nb} = q_w - q_{conv,2ph}. \tag{11}$$

Herein, the convective component $q_{conv,2ph}$ is computed in terms of an enhanced single-phase convection $q_{conv,1ph}$ using the Colburn analogy between the wall heat transfer and the wall friction to describe the enhancement, so that one may write

$$q_{conv,2ph} = q_{conv,1ph}\left(\frac{u_{\tau,2ph}}{u_{\tau,1ph}}\right)^2. \tag{12}$$

The ratio $(u_{\tau,\ 2ph}/u_{\tau,\ 1ph})^2$ is determined from the experimental data by relating the measured wall friction velocities for the bubble-laden two-phase cases to those measured in the corresponding bubble-free single-phase cases. The convective single-phase heat flux $q_{conv,1ph}$ in Eq. (12) is computed as

$$q_{conv,1ph} = \alpha_{conv,1ph}(T_w - T_b), \tag{13}$$

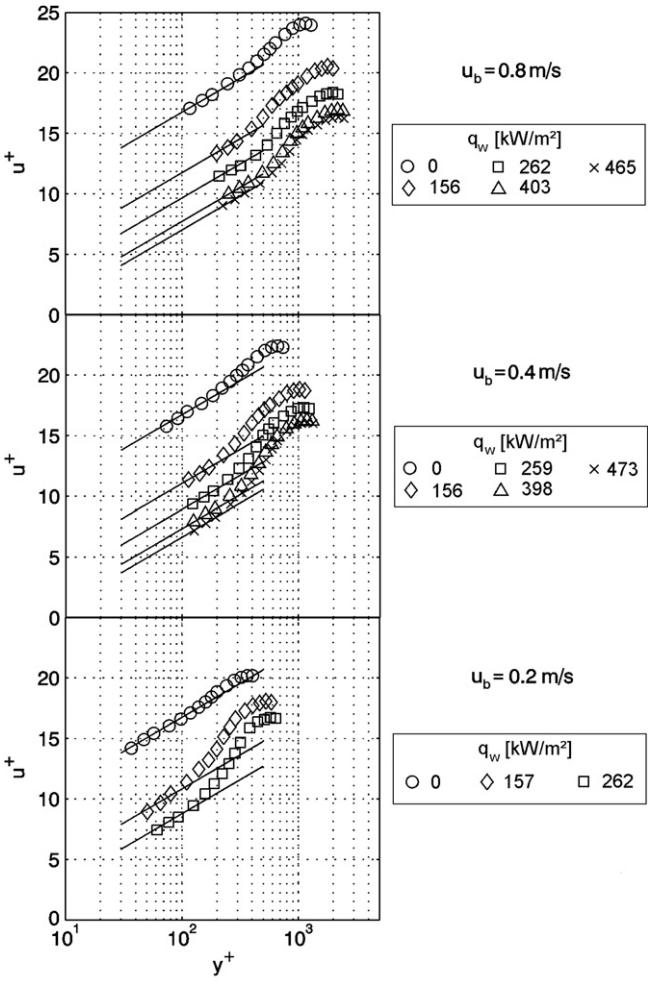

Fig. 8. The logarithmic law of the wall (Eq. (8)) compared to the measured velocity profiles in wall units for different bulk velocities u_b and wall heat fluxes q_w. Solid line, "—", log-law for rough surfaces.

where the heat transfer coefficient $\alpha_{conv,1ph}$ is obtained from the experimental $q_w - T_w$ data of the single-phase cases ($T_w < T_{sat}$).

4.2. Total wall heat flux

In the proposed roughness model, the computation of the wall heat flux is coupled with the calculation of the wall shear stress through the modeled bubble-equivalent roughness height $\tilde{k}_r$. In the present work, the shear stress velocity $u_{\tau,\,2ph}$ is related to the given bulk velocity u_b using the well-established correlation for rough pipes according to Colebrook

$$u_{\tau,2ph} = \sqrt{\frac{\lambda_f}{8}}u_b \quad \text{with}$$

$$\lambda_f = \left[-2\log\left(\frac{2.51}{Re\sqrt{\lambda_S}} + 0.27C_{krc}\frac{\tilde{k}_r}{D_h}\right)\right]^{-2}, \tag{14}$$

which incorporates the modeled bubble-equivalent roughness height $\tilde{k}_r$. The roughness topology dependent parameter C_{krc} is set to 0.65.

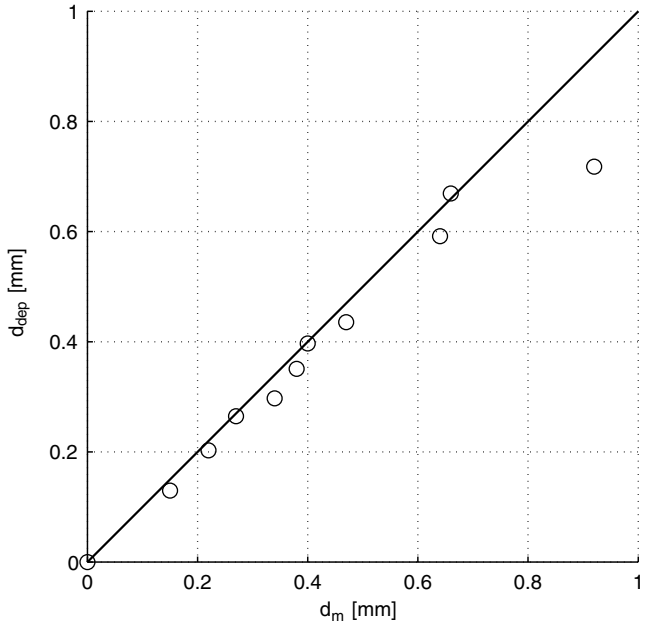

Fig. 9. Bubble departure diameters d_{dep} predicted by the model of Zeng et al. [20] in comparison with our experimental data.

In Figs. 10 and 11, the results for the roughness height $\tilde{k}_r$ and for the shear stress velocity $u_{\tau,\,2ph}$ produced by the model Eqs. (10) and (14), respectively, are compared against the corresponding values for k_r and u_τ, which are associated with the log-law approximations of the measured velocity profiles shown in Fig. 8. The parameters in Eq. (10) were set to $\eta = 2.736$ and $\zeta = 0.1665$. The agreement of the modeled values with the data obtained from the measurements is very good.

As for the computation of the total wall heat flux, the ratio $q_{nb}/\,q_w$ occurring in Eq. (10) suggests the use of a superposition model, since this concept explicitly distinguishes between nucleate boiling and convective contribution. In the present work, two very popular alternative approaches are used: the linear superposition approach introduced by Chen [3], Eq. (3), and the power-additive superposition approach proposed by Steiner and Taborek [12], Eq. (4). In both models, the enhancement factor F_{2ph} in Eq. (3) is computed as

$$F_{2ph} = \frac{q_{conv,2ph}}{q_{conv,1ph}} = \left(\frac{u_{\tau,2ph}}{u_{\tau,1ph}}\right)^2 \tag{15}$$

using Colebrook's formula Eq. (14) for $u_{\tau,\,2ph}$ and $u_{\tau,\,1ph}$, where the latter is associated with a zero bubble-equivalent roughness height $\tilde{k}_r = 0$. The nucleate boiling contribution q_{nb} is obtained using Rohsenow's [7] well-established pool boiling correlation for aqueous liquids

$$q_{nb} = \left(\frac{c}{h_{lg}}\frac{1}{C_{sf}}Pr^{-1}\right)^{1/\gamma}\left(\frac{\sigma}{g(\rho_l - \rho_v)}\right)^{-1/2} h_{fg}\mu_l(T_w - T_{sat})^{1/\gamma} \tag{16}$$

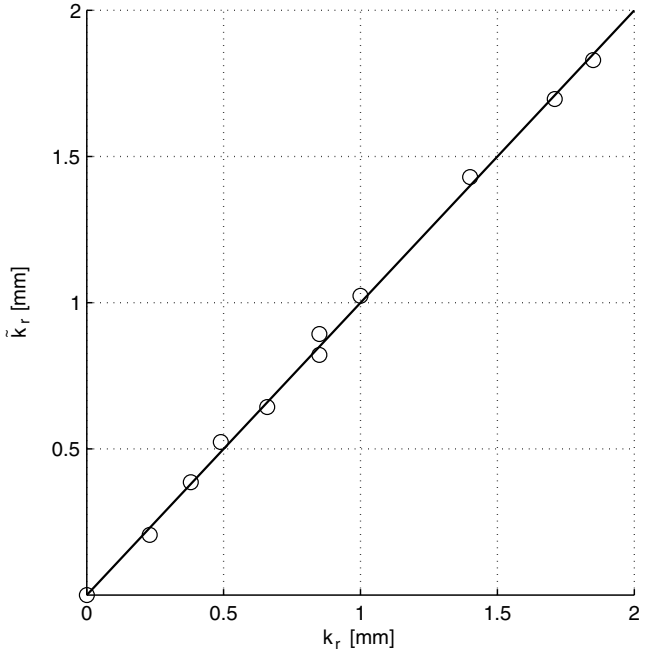

Fig. 10. Predicted bubble-equivalent roughness heights $\tilde{k}_r$ in comparison with experimental data.

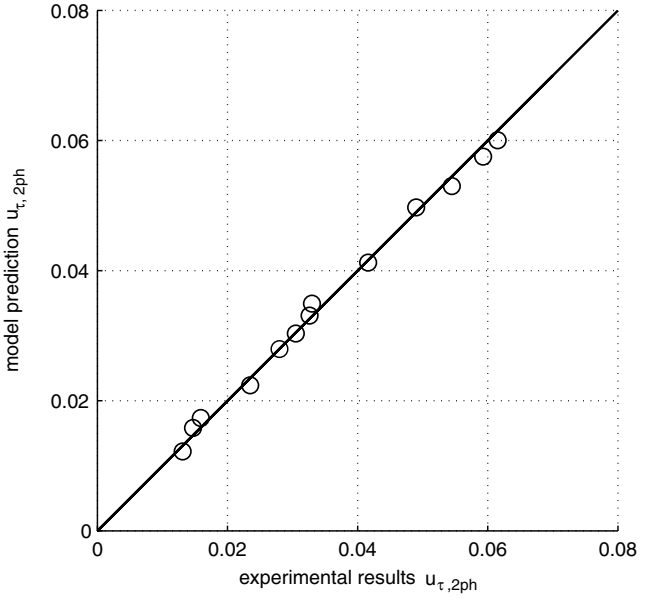

Fig. 11. Predicted shear stress velocities $u_{\tau,\ 2ph}$ in comparison with experimental data.

with the surface-liquid combination dependent parameters $C_{sf} = 0.0167$ and $\gamma = 0.4$. The flow-induced suppression factor needed in Chen's model is computed from the equation

$$S = \left[1 + a\left(ReF_{2ph}^{1.25}\right)^{b}\right]^{-1}, \tag{17}$$

which involves the bulk Reynolds number Re and model constants $a = 5 \times 10^{-6}$ and $b = 1.08$. The exponent occurring in the power-additive superposition model, Eq. (4), was set to $m = 1.6$.

The predicted boiling curves obtained with both superposition models, Eqs. (3) and (4), are shown in Figs. 12 and 13, respectively. Both approaches exhibit a good overall agreement with measurements represented by the symbols. The asymptotic limits, i.e., the straight single-phase convection lines (dash-dotted lines 1′–4′), and the pool boiling curve given by Eq. (16) (dotted line) are also shown in Figs. 12 and 13. This makes the basic idea behind the superposition approach obvious, which constructs the total wall heat flux q_w as a weighted linear or non-linear combination of the two asymptotic solutions. The convergence of the individual boiling curves at high wall superheats towards the pool boiling limit is ensured by incorporating a suppression factor S in the linear case, while it is ensured by setting the exponent $m > 1$ in the non-linear case. The enhanced convective contributions $q_{conv,2ph}$ (dashed lines 1″–4″) predicted by the roughness model tend to make up a substantial part of the total wall heat flux q_w, especially for high bulk velocities. The capability of the roughness model to account for the influence of the bubbles on the dynamic boundary condition in terms of an increased shear stress velocity $u_{\tau,\ 2ph}$, as it was demonstrated in Fig. 11, has

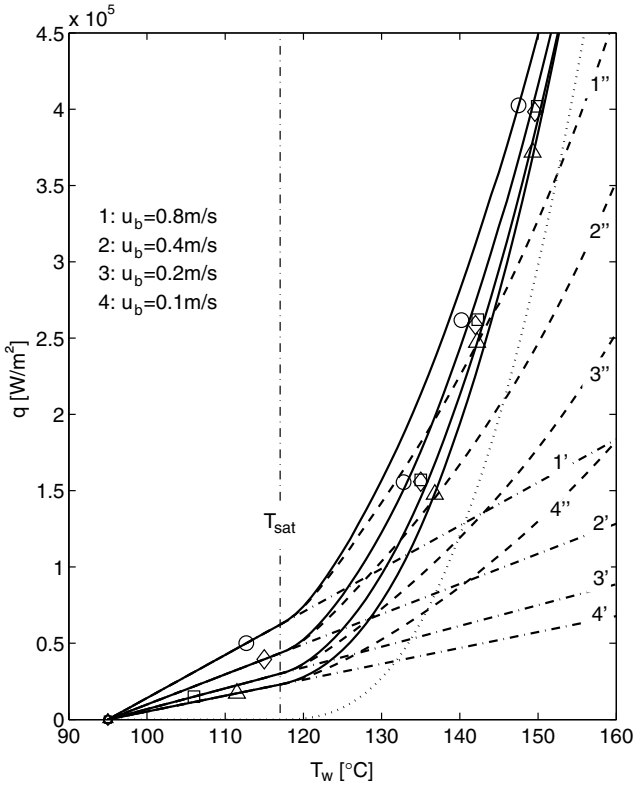

Fig. 12. Predicted flow boiling curves using the linear superposition approach according to Eq. (3) at different velocities of the bulk flow: solid line, "—", total wall heat flux q_w; dash-dotted line, "–·–·–", single-phase convective heat flux $q_{conv,1ph}$; dashed line, "– – –", two-phase convective heat flux $q_{conv,2ph}$, dotted line, "···", pool boiling contribution q_{nb} according to Eq. (16); the symbols denote the measurement data for the four different bulk flow velocities.

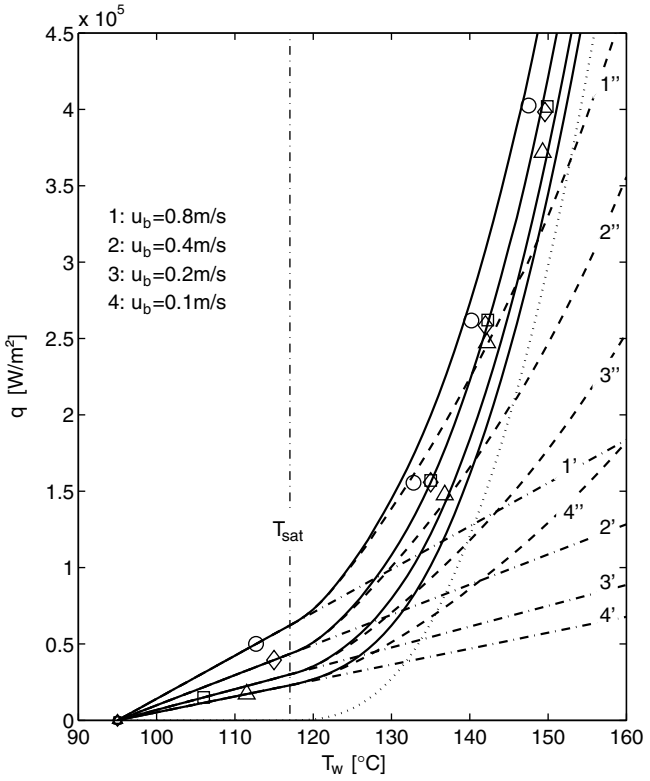

Fig. 13. Predicted flow boiling curves using the power-additive approach according to Eq. (4) at different velocities of the bulk flow: solid line, "—", total wall heat flux q_w; dash-dotted line, "–·–·–", single-phase convective heat flux $q_{conv,1ph}$; dashed line, "– – –", two-phase convective heat flux $q_{conv,2ph}$, dotted line, "···", pool boiling contribution q_{nb} according to Eq. (16); the symbols denote the measurement data for the four different bulk flow velocities.

evidently a strong effect on the weight of the superimposed components of the total wall heat flux. The enhanced convective contribution $q_{conv,2ph}$ relative to the single-phase component $q_{conv,1ph}$ indicates that the present modeling concept can reflect the increased convective heat transfer (bubble-induced microconvection) associated with the experimentally observed increased turbulence in the bubble-laden wall layer (see Figs. 4 and 5). As such, the roughness model enables the single-fluid concept to mimic a characteristic feature of the two-phase heat transfer.

5. Limits of the proposed model

The present model presumes the applicability of the standard logarithmic law of the wall used for turbulent near-wall flow over rough surfaces. As seen from Figs. 4 and 5, this assumption is clearly violated for low bulk velocities ($u_b = 0.1$ m/s and $u_b = 0.2$ m/s) at high wall superheats. Under these conditions, a significant plateau is observed in the measured mean velocity profiles in the streamwise direction $\bar{u}(y)$, as shown in Figs. 4a and 5a above. This observed plateau makes any log-law formulation impossible. It can be attributed to the fact that, at low liquid velocities, the bubbles induce a considerable vertical liquid motion, so that the liquid velocity components in the vertical and the streamwise directions assume the same order of magnitude. It was found that the occurrence of such a plateau can be described as mainly dependent on two non-dimensional parameters, the Froude number

$$Fr = \frac{u_b^2}{g d_{dep}} \tag{18}$$

and the Jakob number

$$Ja = \frac{\rho_l c (T_w - T_{sat})}{\rho_v h_{fg}}. \tag{19}$$

The Froude number based on the bulk velocity u_b and the departure diameter d_{dep} of the bubbles represents the ratio of the streamwise to the bubble-driven vertical momentum fluxes, while the Jakob number essentially represents the influence of the wall superheat. The experimental data were non-dimensionalized and introduced into a nomogram of the Jakob number vs. the Froude number shown in Fig. 14. Some additional cases for bulk velocities $u_b = 0.15$ m/s and $u_b = 0.3$ m/s, respectively, were introduced as well to provide a more complete data base. Data points with the same bulk velocity are connected by dotted lines. The circles denote data points with a plateau in the mean velocity profiles in the streamwise direction. The squares denote the data points without a plateau in the velocity profiles, where the logarithmic law of the wall for rough surfaces is applicable. This region is termed here the buoyancy-independent regime. A demarcation curve (dashed line), which separates the buoyancy-independent from the buoyancy-dependent regime, was found empirically and is represented by the equation

$$Fr = [1 - 0.47 \log(Ja)]^{-1}. \tag{20}$$

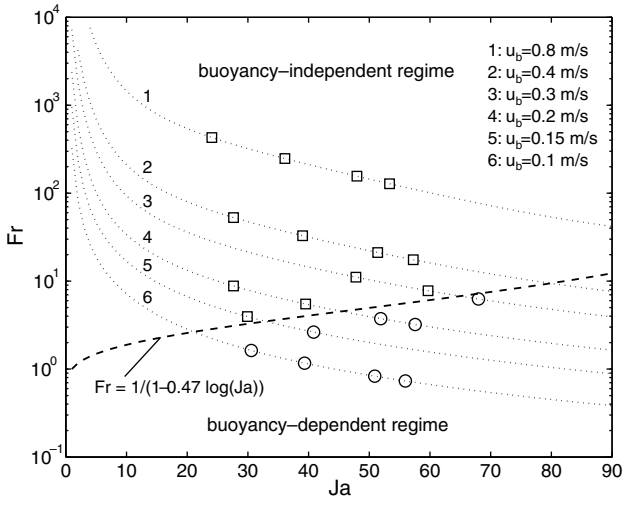

Fig. 14. *Ja–Fr* nomogram for different bulk velocities (dotted lines). The circles ○ denote the measured conditions in the buoyancy-dependent regime; the squares □ denote the measured conditions in the buoyancy-independent regime. The dashed line is the demarcation curve separating the two regimes found empirically.

It becomes very evident that the transition from the buoyancy-independent regime to the buoyancy-dependent regime needs an even higher wall superheat (i.e., Jakob number), the higher the bulk velocity is.

It is noted that the limit represented by the demarcation line Eq. (20) is mainly of relevance for the description of the near-wall velocity field, while its relevance for the prediction of the total wall heat flux is quite small. As seen from Figs. 12 and 13, where all cases of the buoyancy-dependent regime are included as well ($u_b = 0.1$ m/s and $u_b = 0.2$ m/s), the corresponding predictions for the total wall heat flux are not significantly less accurate. This insensitivity to a possibly erroneously predicted microconvective heat transport can be explained by the fact that, in the buoyancy-dependent regime, the total wall heat flux mainly consists of the nucleate boiling contribution to the total wall heat flux and, hence, the convective contribution plays a minor role.

6. Conclusions

Subcooled flow boiling experiments were carried out in a horizontal test channel in order to investigate the near-wall liquid motion under the influence of the vapor bubbles. High-speed camera recordings of the two-phase region were made to gain insight into the size and dynamics of the bubbles. A 2D laser-Doppler anemometer was used to measure the near-wall liquid velocity field. The velocity measurements revealed two main effects of the bubbles. First, the streamwise component is generally decelerated, while the wall-normal component is enhanced. At low liquid Reynolds numbers, the buoyancy-driven motion of the bubbles may become so dominant that a plateau in the mean axial velocity profile is formed. Secondly, it was observed that the turbulent velocity fluctuations are significantly enhanced in the bubble populated region.

Seeking for an appropriate mathematical description of the near-wall streamwise velocity within the framework of single-fluid modeling, it was found that the velocity profiles without plateau follow approximately a log-law for turbulent single-phase flow over rough surfaces. Based on these findings, a model was proposed which captures the influence of the bubbles on the liquid flow in analogy to a surface roughness effect. The proposed model introduces a bubble-equivalent roughness height, which is correlated as dependent on the bubble size and the nucleate boiling contribution to the total wall heat flux. Since the predicted wall shear stress is linked to the wall heat flux through the bubble-equivalent roughness height, the model requires a coupled computation of the dynamic and the thermal boundary conditions in an iterative procedure. Two alternative submodels for the total wall heat flux (a linear and a non-linear superposition approach) gave predictions for the wall friction velocity and the wall heat flux, which are in good agreement with experimental data. An analysis of the individual contributions to the total wall heat flux proved the model capable to reflect the enhanced microconvective momentum and heat transfer caused by the presence of the bubbles in the superheated boundary layer.

At low Reynolds numbers, the proposed model reaches its limit, since the near-wall streamwise velocity cannot be represented adequately by a log-law formulation. A non-dimensional criterion for this limitation was specified. Nonetheless, even beyond this limit, the model was proven to still produce accurate predictions for the total wall heat flux. In these cases, the total wall heat flux mainly consists of the nucleate boiling contribution, so that the error introduced by the model into the convective contribution is comparatively small.

Summing up, it can be concluded that, within the framework of a single-fluid modeling, the proposed approach represents a simple, but efficient method to account for the dynamic effect of vapor bubbles on the near-wall liquid flow field, yielding improved dynamic as well as thermal boundary conditions.

Acknowledgments

Financial support of this work from the K plus Competence Center Program initiated by the Austrian Federal Ministry of Transport, Innovation, and Technology (BMVIT) and funded by FFG, Land Steiermark and Steirische Wirtschaftsförderung (SFG) is gratefully acknowledged. We are also grateful for financial support from AVL List GmbH Graz.

References

[1] S.G. Kandlikar, Heat transfer characteristics in partial boiling, fully developed boiling, and significant void flow regions of subcooled flow boiling, Trans. ASME J. Heat Transfer 120 (1998) 395–401.
[2] M. Shah, A general correlation for heat transfer during subcooled boiling in pipes and annuli, ASHRAE Trans. 83 (Part 1) (1977) 205–217.
[3] J.C. Chen, A correlation for boiling heat transfer to saturated fluids in convective flow, in: ASME preprint 63 HT34 presented at the Sixth National Heat Transfer Conference, Boston, 1963.
[4] H.K. Forster, N. Zuber, Dynamics of vapor bubbles and boiling heat transfer, AIChE J. 1 (1955) 531–535.
[5] M.G. Cooper, Nucleate pool boiling using reduced properties, Adv. Heat Transfer 16 (1984) 157–239.
[6] D. Gorenflo, Behältersieden, VDI Wärmeatlas, VDI Verlag Düsseldorf, 1988, Sec. Ha.
[7] W.M. Rohsenow, A method of correlating heat transfer data for surface boiling of liquids, Trans. ASME 74 (1952) 969–975.
[8] N.A.F. Campbell, J.G. Hawley, K. Robinson, S. Joyce, M. Haigh, Predictions for nucleate boiling – results from a thermal bench marking exercise at low flows, SAE Congress, Paper No. 2002-01-1028, Detroit, 2002.
[9] U. Wenzel, H. Müller-Steinhagen, Heat transfer to mixtures of acetone, isopropanol and water under subcooled flow boiling conditions – II. Predictions of heat transfer coefficients, Int. J. Heat Mass Transfer 33 (1994) 185–194.
[10] H. Steiner, A. Kobor, L. Gebhard, A wall heat transfer model for subcooled boiling flow, Int. J. Heat Mass Transfer 48 (2005) 4161–4173.
[11] Z. Liu, R.H.S. Winterton, A general correlation for saturated and subcooled flow boiling in tubes and annuli based on a nucleate boiling equation, Int. J. Heat Mass Transfer 34 (1991) 2759–2766.

[12] S.S. Kutateladze, Fundamentals of Heat Transfer, Edward Arnold, London, 1963.
[13] D. Steiner, J. Taborek, Flow boiling heat transfer in vertical tubes correlated by an asymptotic model, Heat Transfer Eng. 13 (1992) 43–69.
[14] R. Maurus, Bestimmung des Blasenverhaltens beim unterkühlten Strömungssieden mit der digitalen Bildfolgenanalyse, PhD thesis, Munich University of Technology, 2003.
[15] R. Mei, J.F. Klausner, C.J. Lawrence, A note on the history force on a spherical bubble at finite Reynolds number, Phys. Fluids 6 (1994) 418–420.
[16] A.A. Troshko, Y.A. Hassan, Law of the wall for two-phase turbulent boundary layers, Int. J. Heat Mass Transfer 44 (2001) 871–875.
[17] D. Mikielewicz, Hydrodynamics and heat transfer in bubbly flow in the turbulent boundary layer, Int. J. Heat Mass Transfer 46 (2003) 207–220.
[18] C. Gabillet, C. Colin, J. Fabre, Experimental study of bubble injection in a turbulent boundary layer, Int. J. Multiphase Flow 28 (2002) 553–578.
[19] T. Cebeci, P. Bradshaw, Momentum Transfer in Boundary Layers, Hemisphere, Washington, DC, 1977.
[20] L.Z. Zeng, J.F. Klausner, D.M. Bernhard, R. Mei, A unified model for the prediction of bubble detachment diameters in boiling systems – II. Flow boiling, Int. J. Heat Mass Transfer 36 (1993) 2271–2279.